Brief Communication

Cell Chemical Biology

Activity-based, bioorthogonal imaging of phospholipase D reveals spatiotemporal dynamics of GPCR-Gq signaling

Graphical abstract

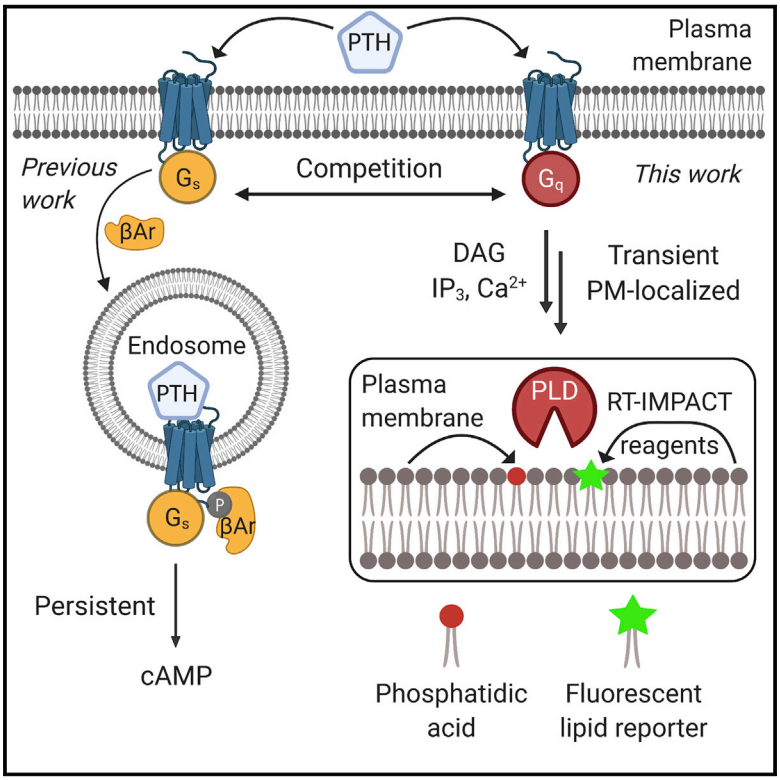

Highlights

- RT-IMPACT is an activity-based method to image phospholipase D signaling
- RT-IMPACT specifically visualizes G_q signaling downstream of PTHR1 activation
- PTHR1 signals via G_q transiently and at the plasma membrane, in contrast to G_s
- Bioorthogonal tools for imaging PLDs are useful probes to image GPCR-G_q signaling

Authors

Dongjun Liang, Ross W. Cheloha, Tomoyuki Watanabe, Thomas J. Gardella, Jeremy M. Baskin

Correspondence

jeremy.baskin@cornell.edu

In brief

The parathyroid hormone receptor (PTHR1) signals via both G_s and G_q, with the former occurring, non-classically, on endosomes. Here, Liang et al. apply a bioorthogonal method for visualizing phospholipase D signaling to reveal that PTHR1-G_q signaling is transient and localized exclusively at the plasma membrane.

Liang et al., 2022, Cell Chemical Biology 29, 67–73
January 20, 2022
https://doi.org/10.1016/j.chembiol.2021.05.020

CellPress

Cell Chemical Biology

CellPress

Brief Communication

Activity-based, bioorthogonal imaging of phospholipase D reveals spatiotemporal dynamics of GPCR-Gq signaling

Dongjun Liang,[1] Ross W. Cheloha,[2] Tomoyuki Watanabe,[3,4] Thomas J. Gardella,[3] and Jeremy M. Baskin[1,5,*]
[1]Department of Chemistry and Chemical Biology and Weill Institute for Cell and Molecular Biology, Cornell University, Ithaca, NY, USA
[2]Chemical Biology in Signaling Section, Laboratory of Bioorganic Chemistry, National Institute of Diabetes and Digestive and Kidney Diseases, Bethesda, MD, USA
[3]Endocrine Unit, Massachusetts General Hospital and Harvard Medical School, Boston, MA, USA
[4]Present address: Chugai Pharmaceutical Company, Japan
[5]Lead contact
*Correspondence: jeremy.baskin@cornell.edu
https://doi.org/10.1016/j.chembiol.2021.05.020

SUMMARY

Canonically, G-protein-coupled receptor (GPCR) signaling is transient and confined to the plasma membrane (PM). Deviating from this paradigm, the parathyroid hormone receptor (PTHR1) stimulates sustained G_s signaling at endosomes. In addition to G_s, PTHR1 activates G_q signaling; yet, in contrast to the PTHR1-G_s pathway, the spatiotemporal dynamics of the G_q branch of PTHR1 signaling and its relationship to G_s signaling remain largely ill defined. Recognizing that a downstream consequence of G_q signaling is the activation of phospholipase D (PLD) enzymes, we leverage activity-based, bioorthogonal imaging tools for PLD signaling to visualize and quantify the G_q branch of PTHR1 signaling. We establish that PTHR1-G_q signaling is short lived, exclusively at the PM, and antagonized by PTHR1 endocytosis. Our data support a model wherein G_q and G_s compete for ligand-bound receptors at the PM and more broadly highlight the utility of bioorthogonal tools for imaging PLDs as probes to visualize GPCR-G_q signaling.

INTRODUCTION

The traditional paradigm for G-protein-coupled receptor (GPCR) signaling involves transient, agonist-induced activation of heterotrimeric G proteins and second-messenger production at the plasma membrane (PM), which terminates upon receptor internalization (Irannejad and Von Zastrow, 2014; L. Mohan et al., 2013; Pavlos and Friedman, 2017). Classically, different second messengers are produced at the PM depending on the Gα subtype that is activated. For example, G_s activates adenylyl cyclase, producing cyclic AMP (cAMP), leading to protein kinase A signaling, whereas $G_{q/11}$ stimulates phospholipase Cβ (PLCβ) enzymes, inducing $PI(4,5)P_2$ hydrolysis to produce diacylglycerol (DAG) and inositol trisphosphate (IP_3), leading to protein kinase C (PKC) and Ca^{2+} signaling. Both G_s and G_q are primarily found in the cytosolic leaflet of the PM, though they can also be found at intracellular locations, along with downstream signaling proteins and second messengers (Marrari et al., 2007; Mohammad Nezhady et al., 2020).

Notably, recent work has identified that certain GPCRs, including opioid receptors (Stoeber et al., 2018), the β_2-adrenergic receptor (β_2AR) (Irannejad et al., 2013), and the parathyroid hormone receptor 1 (PTHR1) (Cheloha et al., 2015; Ferrandon et al., 2009; Sutkeviciute et al., 2019), also signal, via G_s, from intracellular membranes after receptor-mediated endocytosis. In the case of PTHR1, such signaling occurs on endosomes following β-arrestin-induced, clathrin-mediated endocytosis of the ligand-bound GPCR (Luttrell and Lefkowitz, 2002). This non-classical, endosomal signaling persists until V-ATPase-mediated endosomal acidification causes ligand dissociation, and subsequent receptor binding to the retromer complex enables eventual recycling to the PM (Feinstein et al., 2011; Gidon et al., 2014; Vilardaga et al., 2012; Wehbi et al., 2013). Recent efforts to characterize whether GPCRs remain signaling competent after internalization have used single-domain antibodies that bind to the receptor in its active conformation as biosensors (Cheloha et al., 2020a). Although this approach reveals the subcellular localization of GPCRs in their active conformations, it does not elucidate whether these GPCRs maintain the ability to signal via different pathways following internalization.

Sustained endosomal G_s signaling by both β_2AR and PTHR1 has proven physiologically significant for regulating distinct outcomes compared with when confined at the PM (Tsvetanova and von Zastrow, 2014; White et al., 2019). However, PTHR1, which has numerous functions in the physiology of bone, kidney, and other tissues, has a more complex signaling landscape (Sato et al., 2020; Wein and Kronenberg, 2018). In addition to both PM- and endosome-localized G_s-cAMP signaling, PTHR1 also activates the G_q-PLC axis, and such signaling is also physiologically relevant (Abou-Samra et al., 1992; Guo et al., 2002). A long-standing question has been the extent of interplay between the G_q and the G_s branches of PTHR1 signaling, which is

fundamental to the understanding of diverse physiological functions under the control of PTHR1. Some evidence suggests that regulation of PTHR1-G_q signaling occurs within the kidney (Capuano et al., 2007). A recent study revealed that G_q signaling was required for subsequent prolonged, intracellular G_s signaling, via a mechanism implicating Gβγ intracellular translocation and activation of PI3Kb (White et al., 2020).

Nevertheless, the spatiotemporal dynamics of PTHR1-G_q signaling and its full relationship to the G_s pathway remain incompletely understood. Here, we establish a chemical toolset for visualizing the G_q branch of GPCR signaling and apply it to elucidate the spatiotemporal dynamics of PTHR1-G_q signaling and clarify its relationship to G_s signaling. Our approach capitalizes upon the recognition that G_q-PLC signaling—via production of DAG and IP_3 to activate conventional PKCs—leads to stimulation of phospholipase D (PLD) enzymes (Figure 1A). PLDs in turn produce phosphatidic acid (PA), a lipid second messenger that engages several effectors to influence membrane trafficking, cytoskeletal dynamics, and signaling (Nelson and Frohman, 2015; Selvy et al., 2011).

We have developed bioorthogonal chemical tools to visualize and quantify PLD activity with organelle-level resolution (Bumpus et al., 2020; Liang et al., 2019). These approaches harness the ability of PLD enzymes, which normally catalyze phosphatidylcholine hydrolysis to produce PA, to also produce phosphatidyl alcohol lipids via transphosphatidylation with exogenous primary alcohols (Brown et al., 2007). Our tools, termed imaging phospholipase D activity with clickable alcohols via transphosphatidylation (IMPACT), use bioorthogonally labeled alcohols as transphosphatidylation substrates, followed by click chemistry tagging of the resultant lipids in live cells with fluorescent groups (Figure 1B) (Liang et al., 2019).

By using an alcohol and click chemistry partner capable of undergoing a rapid and fluorogenic inverse electron-demand Diels-Alder (IEDDA) cycloaddition, such labeling can be performed in real time (RT-IMPACT) (Bumpus et al., 2020; Liang et al., 2019). In RT-IMPACT, the IEDDA-tagged lipids, prior to their trafficking to other organelle membranes, report on the localizations of endogenous PLD activity (Liang et al., 2019). Because of the specific connection between G_q-PLC signaling and PLD activation, we reasoned that RT-IMPACT would enable us to visualize localizations and quantify the extent of PLD activity downstream of PTHR1-G_q signaling, reporting on the spatiotemporal dynamics of this branch of PTHR1 signaling.

Here, we first establish that RT-IMPACT is a selective reporter for PTHR1-G_q signaling, and we show that PTHR1-G_q signaling specifically activates the PLD1 isoform. We then reveal that PLD1 signaling downstream of PTHR1-G_q is transient and occurs exclusively at the PM. The timescale of this signaling matched that of the PM residence of the ligand-bound GPCR, and inhibition of endocytosis prolonged G_q and suppressed G_s signaling. These data suggest that G_q and G_s compete for PTHR1-mediated signaling upon ligand binding at the PM, hence giving rise to maximal levels of cAMP production after the termination of G_q signaling by receptor endocytosis. This work reveals insights into the spatiotemporal control of signaling via different Gα subunits from the same GPCR and highlights how bioorthogonal tools to visualize PLD signaling can act as selective reporters of G_q signaling.

RESULTS AND DISCUSSION

G_q, but not G_s, is required for PLD activation downstream of PTHR1

We began by determining the specificity of RT-IMPACT as a reporter for G_q signaling downstream of PTHR1. During PTHR1 stimulation, we treated cells with a *trans*-cyclooctene alcohol (oxoTCO, Figure 1C), in the presence or absence of PTHR1 ligands, to generate oxoTCO-containing lipids as transphosphatidylation products. After a rinse and IEDDA tagging with a fluorogenic tetrazine-BODIPY (Tz-BODIPY, Figure 1C), we quantified cellular fluorescence by flow cytometry. To stimulate PTHR1, we first used PTH(1–34), comprising the N-terminal fragment of the parathyroid hormone (PTH), which strongly activates all downstream PTHR1-coupled Gα pathways. We found substantial PTH(1–34)-dependent RT-IMPACT labeling (Figure 1D).

To determine whether RT-IMPACT reports on G_q versus G_s signaling, we treated HEK293 cells stably expressing PTHR1 with PTH(1–34)-Trp1, a G_s-biased ligand that induces binding of the receptor exclusively to G_s (Gardella and Vilardaga, 2015), and found that this ligand exhibited only a very minimal activation of PLDs (Figure 1D). Alternatively, we applied PTH(1–34) with YM-254890 (Nishimura et al., 2010; Takasaki et al., 2004), a G_q-selective inhibitor, and found no detectable PLD activity (Figure 1D). These results are consistent with our previous work using these probes to distinguish PTHR1-dependent G_q versus G_s signaling using fluorescence-based Ca^{2+} measurements as a readout (Roszko et al., 2017; Sato et al., 2020). To selectively activate G_q, we expressed PTHR1 in G_s knockout cells, and upon PTH stimulation, found a level of PLD activity comparable to that from PTH-stimulated, PTHR1-expressing wild-type cells (Figures 1E and S1). These data indicate that G_q, and not G_s, is responsible for the activation of PLDs downstream of PTH-PTHR1 signaling, likely via PLCβ enzymes, which hydrolyze $PI(4,5)P_2$ to generate DAG and IP_3 to activate PKCs, which upregulate PLDs.

PTHR1 predominantly activates the PLD1 isoform at the PM

To characterize the nature of the PTHR1-G_q-induced PLD signaling, we used isoform-selective PLD inhibitors to determine which of the two PLD isoforms that generate PA via PC hydrolysis, PLD1 or PLD2, is responsible for PLD activity downstream of PTHR1. Using RT-IMPACT followed by flow cytometry, we found that a PLD1-selective inhibitor (VU0359595, IC_{50}(PLD1) = 3.7 nM; IC_{50}(PLD2) = 6.4 μM) abrogated nearly all of the PTH-induced PLD activity, equivalent to a pan-PLD inhibitor (Figure 2A). By contrast, a PLD2-selective inhibitor (VU0364739, IC_{50}(PLD1) = 1.5 μM; IC_{50}(PLD2) = 20 nM) had only a modest effect (Figure 2A). Thus, PLD1 is responsible for the bulk of the PLD activity downstream of PTHR1, consistent with the established role of PLD1 as inducible by activated PKCs (Brown et al., 2007; Hu and Exton, 2003).

We next sought to use RT-IMPACT to reveal the subcellular localization of the PTHR1-G_q-induced PLD signaling. Here, we performed a similar RT-IMPACT labeling with oxoTCO during PTH stimulation, rinsing, and then visualization of the fluorogenic IEDDA tagging reaction in real time by time-lapse

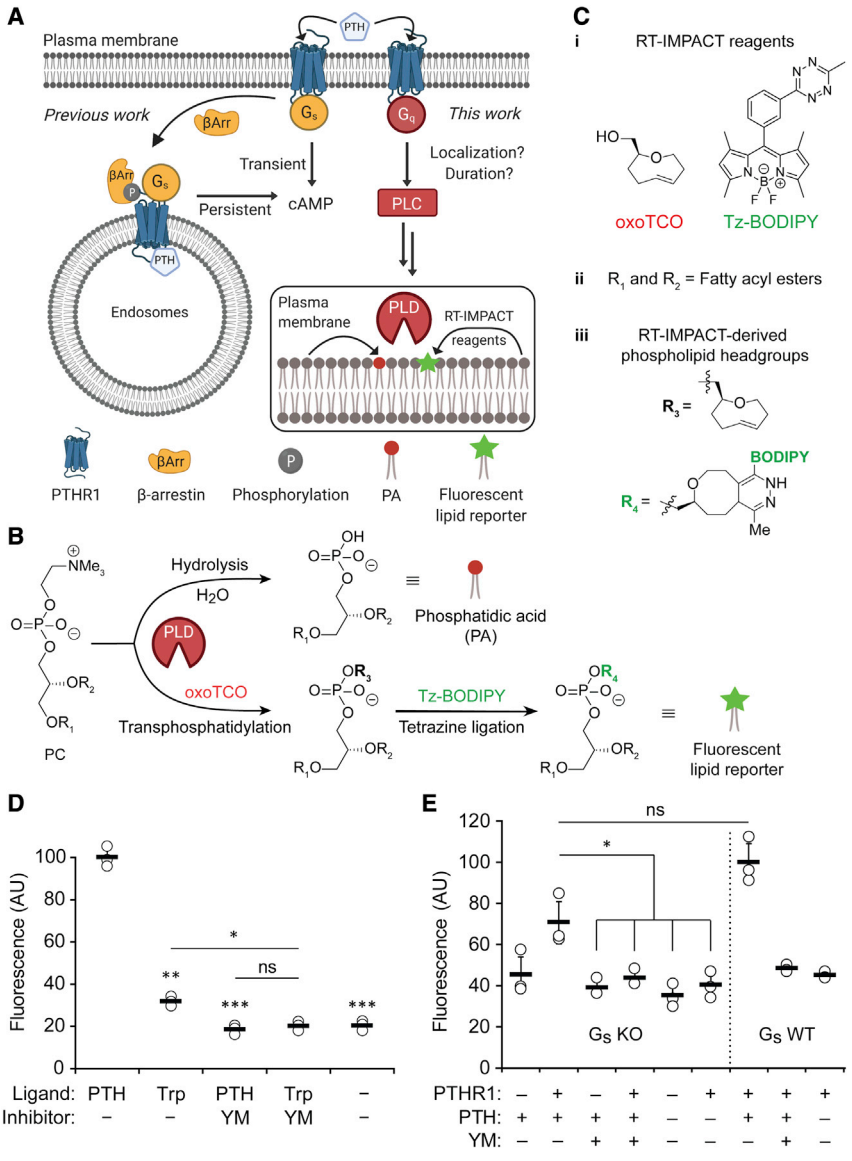

Figure 1. RT-IMPACT is a tool to quantify phospholipase D (PLD) activity elicited by PTHR1-G_q but not PTHR1-G_s signaling

(A) Schematic of PTHR1 signaling, illustrating how RT-IMPACT could report on PTHR-dependent G_q signaling.

(B and C) Schematic of (B) and chemical structures for (C) RT-IMPACT, a tool to visualize endogenous PLD signaling.

(D and E) Flow cytometry of HEK293 cells indicating that RT-IMPACT labeling depends upon PTHR1-G_q signaling. (D) HEK293 cells stably expressing PTHR1 (hPTHR1-293) were incubated with oxoTCO and the indicated PTHR1 ligand for 5 min prior to a rinse and addition of Tz-BODIPY for 1 min, rinse, and flow cytometry analysis. The mean BODIPY fluorescence is shown (AU, arbitrary units). Where indicated, cells were treated with the G_q inhibitor YM-254890 (YM) or DMSO vehicle for 15 min prior to and during the oxoTCO and PTHR1 activation step. PTH, PTH(1–34); Trp (G_s-selective agonist), PTH-Trp. (E) G_s knockout (KO) cells transfected with hPTHR1-HA were stained with AF647-conjugated α-PTHR1 antibody to identify transfected cells. Cells were labeled via RT-IMPACT as in (D). Flow cytometry was performed, gating on PTHR1-positive or -negative cells (left). The mean BODIPY fluorescence is shown. hPTHR1-293 cells (G_s WT) were analyzed concurrently (right). Asterisks above data denote significance compared with PTH without inhibitors. Asterisks above lines denote significance comparing the indicated groups. Error bars represent standard deviation. One-way ANOVA, Games-Howell *post hoc* test: *$p < 0.05$, **$p < 0.01$, and ***$p < 0.001$; ns, not significant; $n = 3$ for (D) and (E).

See also Figure S1.

confocal microscopy. Because of the rapid kinetics of this IEDDA reaction, we could detect its fluorescent lipid products within seconds of administering Tz-BODIPY to the cells, and such images reveal the localization of PLD-generated lipids prior to their subsequent trafficking. Using this technique, we found that PTHR1-induced PLD activity is exclusively at the PM (Figures 2B and S2).

We have previously shown that platelet-derived growth factor receptor signaling induced PLD activity at intracellular membranes using RT-IMPACT (Liang et al., 2019). Therefore, a lack of similar intracellular fluorescence following PTHR1 activation provides strong evidence of a restricted subcellular localization of PLD1 activation in this context. Although PLD1 localizes to many intracellular sites, it can translocate to the PM upon certain stimuli. In this setting, PTHR1-G_q signaling, which activates PLCβ to generate the PKC agonist DAG, would be expected to stimulate the activity of PLDs in this membrane.

RT-IMPACT reveals that PTHR1-G_q activation of PLDs is transient

In addition to the spatial aspects of PTHR1-G_q signaling, we also sought to use RT-IMPACT to elucidate the temporal dynamics of this pathway. The temporal resolution of RT-IMPACT is roughly 5 min, encompassing transphosphatidylation, rinsing, and IEDDA reaction. To quantify PTHR1-G_q signaling elicited by PTH agonism over time, we varied the time after PTH addition prior to oxoTCO addition by 5-min intervals. Flow cytometry of cells labeled via RT-IMPACT in this manner revealed that PLD activity downstream of PTHR1-G_q signaling was transient, peaking within the first 5 min, and rapidly returned to basal levels within 10 min of exposure to PTH (Figures 3A and S3). This finding aligns with previous work showing that PTHR1-G_q signaling induces a transient release of calcium into the cytoplasm that reverts to basal levels within a few minutes (Cheloha et al., 2020b; Sato et al., 2020).

By contrast, PTHR1-G_s signaling was, as expected, delayed and sustained, peaking at 15 min post-PTH application and persisting for at least 60 min, as measured by a cAMP-based biosensor assay (Figure 3B) (Binkowski et al., 2011). This short-lived G_q activation is in line with the classical model of GPCR signaling, wherein ligand-bound receptors are rapidly phosphorylated and internalized via binding to β-arrestins, which

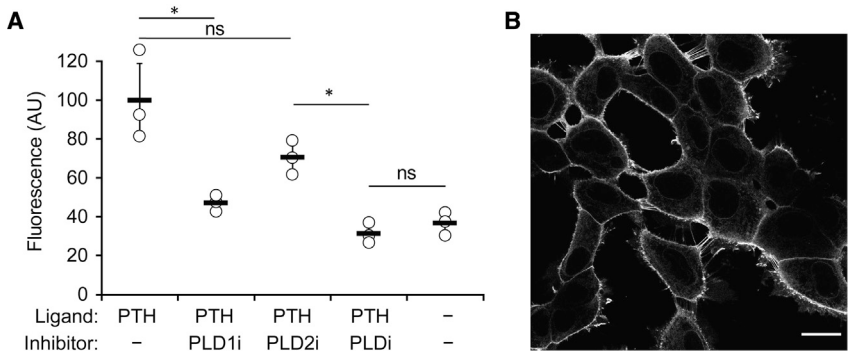

Figure 2. PTHR-G_q-induced PLD signaling is due predominantly to the PLD1 isoform and is localized at the PM

(A) Flow cytometry of PLD activity of hPTHR1-293 cells stimulated by PTH in the presence of pan- or isoform-selective PLD inhibitors. Cells were incubated with the indicated inhibitors (PLD1i, PLD1-selective VU0359595; PLD2i, PLD2-selective VU0364739; PLDi, pan-inhibitor FIPI) or DMSO for 30 min. PTH and oxoTCO were added for 5 min before rinsing, Tz-BODIPY addition, and flow cytometry analysis. Asterisks above lines denote significance comparing the indicated groups. Error bars represent standard deviation. One-way ANOVA, Games-Howell *post hoc* test: *$p < 0.05$; ns, not significant; $n = 3$.

(B) Confocal microscopy of hPTHR1-293 cells stimulated with PTH and labeled via RT-IMPACT to reveal localization of PTHR1-derived PLD signaling, showing 9 s post-addition of Tz-BODIPY. Scale bar: 20 μm.

See also Figure S2.

terminates most GPCR signaling processes but prolongs G_s signaling in the case of PTHR1.

Despite such rapid deactivation of PTHR1-G_q signaling within 10 min of PTH stimulation, the observed PLD activity at various time points (1, 2, and 5 min) post-addition of either PTH or rhodamine-tagged PTH (PTH-TMR), to visualize PTH-PTHR1 complexes, was predominantly at the PM even before complete desensitization (Figure S2), suggesting that G_q activation of PLD was confined to the PM in this context. Importantly, our findings reinforce and are complementary to a recent report that G_q activation is critical for prolonged endosomal G_s signaling through the recruitment of β-arrestins (White et al., 2020).

Receptor endocytosis antagonizes PTHR1-G_q-elicited PLD activity

The above data reveal a stark contrast between the spatiotemporal dynamics of PTHR1-induced G_q and G_s signaling, with the former transient and at the PM and the latter being sustained and largely from endosomes (Feinstein et al., 2011). Typically, ligand-bound GPCRs are internalized via interaction with β-arrestin and subsequent clathrin-mediated endocytosis (Lefkowitz, 1998; Shukla et al., 2011). We hypothesized that receptor-mediated endocytosis might act as a key control point for the switch from G_q to G_s signaling (Feinstein et al., 2011). To test this idea, we perturbed the endocytosis of PTHR1 and investigated the effects on the amplitudes and kinetics of G_q and G_s signaling.

First, we tested the effects of blocking endocytosis by treating cells with Dyngo-4a, an inhibitor of dynamin (Harper et al., 2011; McCluskey et al., 2013; Tsvetanova and von Zastrow, 2014), a GTPase required for clathrin-mediated endocytosis. We established conditions under which Dyngo-4a reduced the endocytosis of PTHR1, by visualizing PTH-PTHR1 complexes by confocal microscopy in cells treated with PTH-TMR. At 5–10 min after PTH-TMR addition, we found that Dyngo-4a led to substantially reduced internalization of PTHR1-PTH-TMR complexes (Figure 4A). We then found that Dyngo-4a treatment led to prolonged G_q activation compared with control, as assessed by flow cytometry of RT-IMPACT-labeled cells (Figure 4B). By contrast, under these same conditions, the magnitude of PTHR1-G_s signaling was significantly reduced (Figure 4C). Moreover, the same inhibitory effect of Dyngo-4a on G_s signaling was confirmed in human osteosarcoma cells, which express physiological levels of PTHR1 (Figure S4A), although we were unable to detect Ca^{2+} responses by fura-2 or PLD activity by IMPACT, following PTH stimulation in these cells, speaking to a possible combination of factors, including a limited sensitivity of the method, low levels of PTHR1 expression, and a more modest stimulation of G_q, compared with G_s, by PTHR1 (Inoue et al., 2019) (Figures S4B and S4C).

To account for any potential off-target effects of Dyngo-4a (Park et al., 2013; Preta et al., 2015), we corroborated these findings by perturbing endocytosis using two independent methods. First, we treated cells with bafilomycin A1 (BafA1), an inhibitor of the V-ATPase responsible for endosomal acidification. Prolonged BafA1 treatment, by preventing endosomal maturation to lysosomes, has the ultimate effect of diminishing endocytosis (Gidon et al., 2014; Kozik et al., 2013). Similar to Dyngo-4a, BafA1 potentiated G_q-induced PLD signaling (Figures S4D and S4E). Alternatively, we perturbed clathrin-mediated endocytosis through acute inhibition of β-arrestins by the pharmacological inhibitor barbadin, which blocks interactions between β-arrestin and the clathrin adaptor protein AP2 to prevent endocytosis of β_2AR (Beautrait et al., 2017). Consistent with the Dyngo-4a and BafA1 experiments, barbadin treatment prolonged PTHR1-dependent PLD activation (Figure S4F).

Collectively, these results support a model wherein the PTHR1-G_q pathway is restricted to the PM. Under physiological conditions, this branch of PTHR1 signaling is short lived and is terminated upon endocytosis of PTHR1, within 5–10 min of ligand binding. By contrast, the G_s-cAMP pathway occurs on both membranes. At the PM, a brief burst of G_s signaling, immediately following PTHR1 activation, has been reported, but the bulk of G_s signaling is now appreciated to occur at early endosomes, peaking at ~15 min and lasting for more than 1 h.

These observations can be explained by a model wherein G_q and G_s compete for binding to PTH-bound PTHR1 receptors at the PM, where both pathways are active upon initial ligand binding (Figure 4D). Phosphorylation and subsequent β-arrestin-mediated

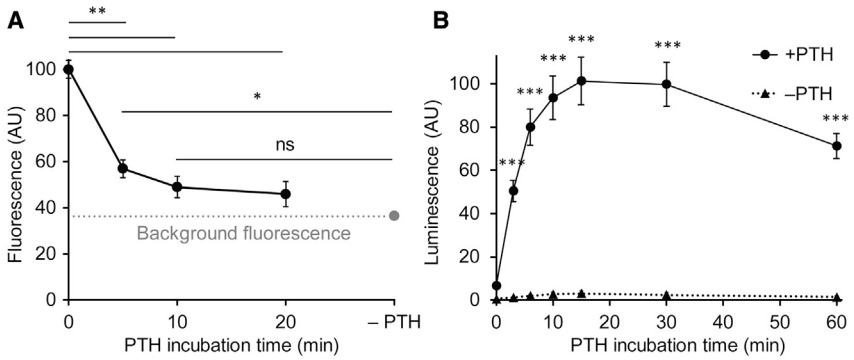

Figure 3. PLD activation downstream of PTHR1-G_q signaling is transient, in contrast to persistent PTHR1-G_s signaling

(A) Flow cytometry of hPTHR1-293 cells, showing extent of PLD activity following PTH addition. hPTHR1-293 cells were stimulated with PTH for 0–20 min, followed by oxoTCO addition for 5 min, rinsing, Tz-BODIPY addition, and flow cytometry. Gray, background fluorescence in the absence of PTH.

(B) Levels of cAMP from hPTHR1-293 cells stably expressing cAMP GloSensor after addition of PTH (solid line; circles) or control (dashed line; triangles). In (A), asterisks above lines denote significance comparing the indicated groups. In (B), asterisks above groups represent significance comparing the ±PTH conditions at each time point. Error bars represent standard deviation. One-way ANOVA, Games-Howell *post hoc* test: *$p < 0.05$, **$p < 0.01$, and ***$p < 0.001$; ns, not significant; n = 3 for (A) and n = 4 for (B).
See also Figure S3.

endocytosis of PTHR1 terminates PTHR1-G_q signaling, leading ultimately to PTHR1 signaling at endosomes via the G_s-cAMP pathway, such that maximal cAMP levels correlate with the termination of G_q-induced PLD signaling. The pharmacological perturbations of receptor endocytosis, which enhance G_q signaling and attenuate G_s signaling, further support this model of a competitive relationship between G_q and G_s signaling in this system.

Conclusion

We have established that RT-IMPACT, an activity-based, bioorthogonal method for visualizing PLD signaling, can be used to selectively image and quantify GPCR-G_q signaling. We applied RT-IMPACT to elucidate the spatiotemporal dynamics of G_q signaling downstream of PTHR1, an important GPCR in physiology and disease that signals through multiple Gα proteins at diverse subcellular locations. Following PTH binding, PLD activity downstream of PTHR1-G_q signaling occurs transiently and exclusively at the PM. Perturbations of receptor endocytosis prolonged such G_q signaling and reduced G_s signaling, which predominantly occurs on endosomes, supporting a model for competition between G_q and G_s for binding to the activated receptor. These data reinforce that G_q and G_s signals downstream of PTHR1 activation exhibit vastly different spatiotemporal behaviors, and such dynamics may be critical for the distinct physiological outcomes of these signaling pathways. More generally, our study highlights the value of applying bioorthogonal imaging methods for tracking PLD activity to understand the regulation of diverse signaling pathways that intersect with PLD signaling.

SIGNIFICANCE

GPCRs can signal via multiple Gα subtypes, and certain GPCRs, including the parathyroid hormone receptor PTHR1, engage in non-classical G_s signaling from endosomes, following their endocytosis. The localization and duration of signaling via other Gα subtypes such as $G_{q/11}$ have remained challenging to determine with traditional approaches. Here, we use bioorthogonal, activity-based tools for visualizing phospholipase D (PLD) signaling as a means to selectively visualize and quantify G_q signaling by PTHR1 and determine that such signaling occurs transiently and exclusively at the plasma membrane, upstream of sustained endosomal G_s signaling. Direct imaging of PLD activation represents a means to reveal the spatiotemporal dynamics of GPCR-G_q signaling.

STAR★METHODS

Detailed methods are provided in the online version of this paper and include the following:

- KEY RESOURCES TABLE
- RESOURCE AVAILABILITY
  - Lead contact
  - Materials availability
  - Data and code availability
- EXPERIMENTAL MODEL AND SUBJECT DETAILS
  - Cell lines
- METHOD DETAILS
  - General materials and methods
  - RT-IMPACT labeling with oxoTCO for live-cell imaging and flow cytometry analysis
  - Luciferase assays of cAMP production
  - Imaging of PTH-TMR to visualize PTHR1 endocytosis
  - RT-IMPACT imaging of the localization of PLD activity
- QUANTIFICATION AND STATISTICAL ANALYSIS

SUPPLEMENTAL INFORMATION

Supplemental information can be found online at https://doi.org/10.1016/j.chembiol.2021.05.020.

ACKNOWLEDGMENTS

J.M.B. acknowledges support from NSF CAREER (CHE-1749919), Beckman Young Investigator, and Sloan Research Fellowship awards. T.J.G. acknowledges support from the NIH (P01DK011794). D.L. was supported by a Cornell Fellowship. R.W.C. was supported by a CRI Irvington Postdoctoral Fellowship. Schematics were created with BioRender.com. We thank the Baskin lab for helpful discussions, Kane Wu for technical assistance, and the Emr, Fromme, and Yu labs for use of equipment.

AUTHOR CONTRIBUTIONS

Conceptualization, D.L., R.W.C., T.J.G., and J.M.B.; investigation, D.L. and T.W.; methodology, D.L. and T.W.; formal analysis, D.L.; visualization, D.L.; writing – original draft, D.L., R.W.C., and J.M.B.; writing – review & editing,

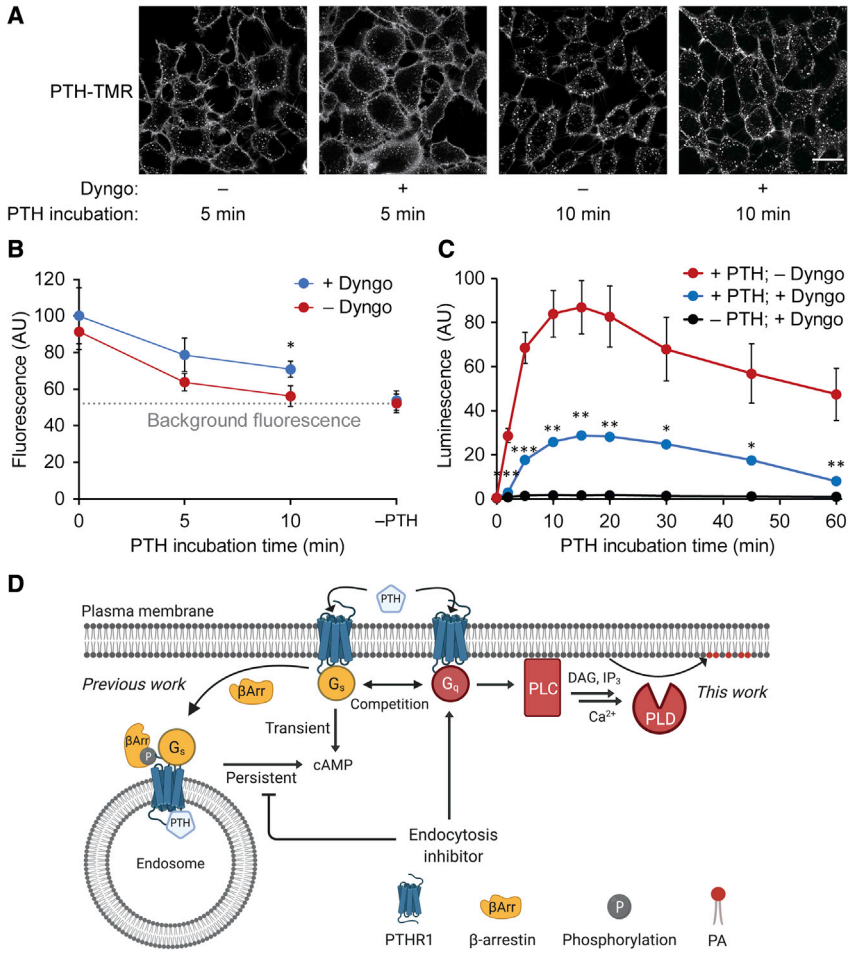

Figure 4. Inhibition of PTHR1 endocytosis prolongs PLD activation through G_q and reduces G_s-cAMP signaling

(A) Confocal microscopy of hPTHR1-293 cells treated with rhodamine-PTH (PTH-TMR) for 5–10 min. Cells were treated with Dyngo-4a or DMSO vehicle 15 min prior to and during ligand addition. Scale bar: 30 μm.

(B) Flow cytometry of hPTHR1-293 cells, showing extent of PLD activity over 20 min after the PTH addition ± Dyngo addition. hPTHR1-293 cells were incubated with Dyngo or vehicle for 15 min, stimulated with PTH for 0–20 min in the presence of Dyngo or vehicle, followed by addition of oxoTCO (5 min) in the presence of PTH and Dyngo or vehicle, rinsing, addition of Tz-BODIPY, and flow cytometry. The mean BODIPY fluorescence is shown. Gray, background fluorescence in the absence of PTH.

(C) Time course of cAMP levels in hPTHR1-293 cells stably expressing cAMP GloSensor. Dyngo or vehicle was added 15 min prior to and during the PTH labeling step.

(D) Model indicating competition between G_q and G_s signaling downstream of PTHR1. In (B and C), asterisks above data denote significance comparing blue and red data points (+ versus – Dyngo in the presence of PTH). Error bars represent standard deviation. One-way ANOVA, Games-Howell *post hoc* test: *$p < 0.05$, **$p < 0.01$, ***$p < 0.001$; $n = 3$ for (B) and $n = 4$ for (C).

See also Figure S4.

D.L., R.W.C., and J.M.B.; project administration, J.M.B.; supervision, J.M.B.; resources, R.W.C.; funding acquisition, T.J.G. and J.M.B.

DECLARATION OF INTERESTS

The authors declare no competing interests.

Received: January 22, 2021
Revised: April 29, 2021
Accepted: May 27, 2021
Published: June 22, 2021

REFERENCES

Abou-Samra, A.B., Juppner, H., Force, T., Freeman, M.W., Kong, X.F., Schipani, E., Urena, P., Richards, J., Bonventre, J.V., Potts, J.T., et al. (1992). Expression cloning of a common receptor for parathyroid hormone and parathyroid hormone-related peptide from rat osteoblast-like cells: a single receptor stimulates intracellular accumulation of both cAMP and inositol trisphosphates and increases intracel. Proc. Natl. Acad. Sci. U S A *89*, 2732–2736.

Beautrait, A., Paradis, J.S., Zimmerman, B., Giubilaro, J., Nikolajev, L., Armando, S., Kobayashi, H., Yamani, L., Namkung, Y., Heydenreich, F.M., et al. (2017). A new inhibitor of the β-arrestin/AP2 endocytic complex reveals interplay between GPCR internalization and signalling. Nat. Commun. *8*, 15054.

Binkowski, B.F., Butler, B.L., Stecha, P.F., Eggers, C.T., Otto, P., Zimmerman, K., Vidugiris, G., Wood, M.G., Encell, L.P., Fan, F., et al. (2011). A luminescent biosensor with increased dynamic range for intracellular cAMP. ACS Chem. Biol. *6*, 1193–1197.

Brown, H.A., Henage, L.G., Preininger, A.M., Xiang, Y., and Exton, J.H. (2007). Biochemical analysis of phospholipase D. Methods Enzymol. *434*, 49–87.

Bumpus, T.W., Liang, D., and Baskin, J.M. (2020). IMPACT: imaging phospholipase D activity with clickable alcohols via transphosphatidylation. Methods Enzymol. *641*, 75–94.

Capuano, P., Bacic, D., Roos, M., Gisler, S.M., Stange, G., Biber, J., Kaissling, B., Weinman, E.J., Shenolikar, S., Wagner, C.A., et al. (2007). Defective coupling of apical PTH receptors to phospholipase C prevents internalization of the Na+-phosphate cotransporter NaP i-IIa in Nherf1-deficient mice. Am. J. Physiol. Cell Physiol. *292*, C927–34.

Cheloha, R.W., Maeda, A., Dean, T., Gardella, T.J., and Gellman, S.H. (2014). Backbone modification of a polypeptide drug alters duration of action in vivo. Nat. Biotechnol. *32*, 653–655.

Cheloha, R.W., Gellman, S.H., Vilardaga, J.P., and Gardella, T.J. (2015). PTH receptor-1 signalling - Mechanistic insights and therapeutic prospects. Nat. Rev. Endocrinol. *11*, 712–724.

Cheloha, R.W., Watanabe, T., Dean, T., Gellman, S.H., and Gardella, T.J. (2016). Backbone modification of a parathyroid hormone receptor-1 antagonist/inverse agonist. ACS Chem. Biol. *11*, 2752–2762.

Cheloha, R.W., Harmand, T.J., Wijne, C., Schwartz, T.U., and Ploegh, H.L. (2020a). Exploring cellular biochemistry with nanobodies. J. Biol. Chem. *295*, 15307–15327.

Cheloha, R.W., Fischer, F.A., Woodham, A.W., Daley, E., Suminski, N., Gardella, T.J., and Ploegh, H.L. (2020b). Improved GPCR ligands from nanobody tethering. Nat. Commun. *11*, 2087.

Daley, E.J., Khatri, A., Dean, T., Vilardaga, J.P., Zaidi, S.A., Katritch, V., and Gardella, T.J. (2021). Ligand-dependent effects of methionine-8 oxidation in parathyroid hormone peptide analogues. Endocrinology *162*, 1–14.

Feinstein, T.N., Wehbi, V.L., Ardura, J.A., Wheeler, D.S., Ferrandon, S., Gardella, T.J., and Vilardaga, J.P. (2011). Retromer terminates the generation of cAMP by internalized PTH receptors. Nat. Chem. Biol. *7*, 278–284.

Ferrandon, S., Feinstein, T.N., Castro, M., Wang, B., Bouley, R., Potts, J.T., Gardella, T.J., and Vilardaga, J.P. (2009). Sustained cyclic AMP production by parathyroid hormone receptor endocytosis. Nat. Chem. Biol. *5*, 734–742.

Gardella, T.J., and Vilardaga, J.P. (2015). International union of basic and clinical pharmacology. XCIII. The parathyroid hormone receptors—family B G protein–coupled receptors. Pharmacol. Rev. *67*, 310–337.

Gidon, A., Al-Bataineh, M.M., Jean-Alphonse, F.G., Stevenson, H.P., Watanabe, T., Louet, C., Khatri, A., Calero, G., Pastor-Soler, N.M., Gardella, T.J., et al. (2014). Endosomal GPCR signaling turned off by negative feedback actions of PKA and v-ATPase. Nat. Chem. Biol. *10*, 707–709.

Guo, J., Chung, U. Il, Kondo, H., Bringhurst, F.R., and Kronenberg, H.M. (2002). The PTH/PTHrP receptor can delay chondrocyte hypertrophy in vivo without activating phospholipase C. Dev. Cell *3*, 183–194.

Harper, C.B., Martin, S., Nguyen, T.H., Daniels, S.J., Lavidis, N.A., Popoff, M.R., Hadzic, G., Mariana, A., Chau, N., McCluskey, A., et al. (2011). Dynamin inhibition blocks botulinum neurotoxin type A endocytosis in neurons and delays botulism. J. Biol. Chem. *286*, 35966–35976.

Hu, T., and Exton, J.H. (2003). Mechanisms of regulation of phospholipase D1 by protein kinase Ca. J. Biol. Chem. *278*, 2348–2355.

Inoue, A., Raimondi, F., Kadji, F.M.N., Singh, G., Kishi, T., Uwamizu, A., Ono, Y., Shinjo, Y., Ishida, S., Arang, N., et al. (2019). Illuminating G-protein-coupling selectivity of GPCRs. Cell *177*, 1933–1947.e25.

Irannejad, R., and Von Zastrow, M. (2014). GPCR signaling along the endocytic pathway. Curr. Opin. Cell Biol. *27*, 109–116.

Irannejad, R., Tomshine, J.C., Tomshine, J.R., Chevalier, M., Mahoney, J.P., Steyaert, J., Rasmussen, S.G.F., Sunahara, R.K., El-Samad, H., Huang, B., et al. (2013). Conformational biosensors reveal GPCR signalling from endosomes. Nature *495*, 534–538.

Kozik, P., Hodson, N.A., Sahlender, D.A., Simecek, N., Soromani, C., Wu, J., Collinson, L.M., and Robinson, M.S. (2013). A human genome-wide screen for regulators of clathrin-coated vesicle formation reveals an unexpected role for the V-ATPase. Nat. Cell Biol. *15*, 50–60.

Lambert, W.D., Scinto, S.L., Dmitrenko, O., Boyd, S.J., Magboo, R., Mehl, R.A., Chin, J.W., Fox, J.M., and Wallace, S. (2017). Computationally guided discovery of a reactive, hydrophilic: trans -5-oxocene dienophile for bioorthogonal labeling. Org. Biomol. Chem. *15*, 6640–6644.

Lefkowitz, R.J. (1998). G protein-coupled receptors: III. New roles for receptor kinases and β- arrestins in receptor signaling and desensitization. J. Biol. Chem. *273*, 18677–18680.

Liang, D., Wu, K., Tei, R., Bumpus, T.W., Ye, J., and Baskin, J.M. (2019). A real-time click chemistry imaging approach reveals stimulus-specific subcellular locations of phospholipase D activity. Proc. Natl. Acad. Sci. U S A *116*, 15453–15462.

Luttrell, L.M., and Lefkowitz, R.J. (2002). The role of β-arrestins in the termination and transduction of G-protein-coupled receptor signals. J. Cell Sci. *115*, 455–465.

Maeda, A., Okazaki, M., Baron, D.M., Dean, T., Khatri, A., Mahon, M., Segawa, H., Abou-Samra, A.B., Jüppner, H., Bloch, K.D., et al. (2013). Critical role of parathyroid hormone (PTH) receptor-1 phosphorylation in regulating acute responses to PTH. Proc. Natl. Acad. Sci. U S A *110*, 5864–5869.

Marrari, Y., Crouthamel, M., Irannejad, R., and Wedegaertner, P.B. (2007). Assembly and trafficking of heterotrimeric G proteins. Biochemistry *46*, 7665–7677.

McCluskey, A., Daniel, J.A., Hadzic, G., Chau, N., Clayton, E.L., Mariana, A., Whiting, A., Gorgani, N.N., Lloyd, J., Quan, A., et al. (2013). Building a better dynasore: the dyngo compounds potently inhibit dynamin and endocytosis. Traffic *14*, 1272–1289.

Mohammad Nezhady, M.A., Rivera, J.C., and Chemtob, S. (2020). Location bias as emerging paradigm in GPCR biology and drug discovery. iScience *23*, 101643.

Mohan, M.L., Vasudevan, N.T., Gupta, M.K., Martelli, E.E., and Naga Prasad, S.V. (2013). G-protein coupled receptor resensitization - appreciating the balancing act of receptor function. Curr. Mol. Pharmacol. *5*, 350–361.

Nelson, R.K., and Frohman, M.A. (2015). Physiological and pathophysiological roles for phospholipase D. J. Lipid Res. *56*, 2229–2237.

Nishimura, A., Kitano, K., Takasaki, J., Taniguchi, M., Mizuno, N., Tago, K., Hakoshima, T., and Itoh, H. (2010). Structural basis for the specific inhibition of heterotrimeric Gq protein by a small molecule. Proc. Natl. Acad. Sci. U S A *107*, 13666–13671.

Park, R.J., Shen, H., Liu, L., Liu, X., Ferguson, S.M., and De Camilli, P. (2013). Dynamin triple knockout cells reveal off target effects of commonly used dynamin inhibitors. J. Cell Sci. *126*, 5305–5312.

Pavlos, N.J., and Friedman, P.A. (2017). GPCR signaling and trafficking: the long and short of it. Trends Endocrinol. Metab. *28*, 213–226.

Preta, G., Cronin, J.G., and Sheldon, I.M. (2015). Dynasore - not just a dynamin inhibitor. Cell Commun. Signal. *13*, 24.

Roszko, K.L., Bi, R., Gorvin, C.M., Bräuner-Osborne, H., Xiong, X.F., Inoue, A., Thakker, R.V., Strømgaard, K., Gardella, T., and Mannstadt, M. (2017). Knockin mouse with mutant Gα11 mimics human inherited hypocalcemia and is rescued by pharmacologic inhibitors. JCI Insight *2*, e91079.

Sato, T., Verma, S., Khatri, A., Dean, T., Goransson, O., Gardella, T.J., and Wein, M.N. (2020). Comparable initial engagement of intracellular signaling pathways by parathyroid hormone receptor ligands teriparatide, abaloparatide, and long-acting PTH. JBMR Plus *5*, e10441.

Selvy, P.E., Lavieri, R.R., Lindsley, C.W., and Brown, H.A. (2011). Phospholipase D: enzymology, functionality, and chemical modulation. Chem. Rev. *111*, 6064–6119.

Shukla, A.K., Xiao, K., and Lefkowitz, R.J. (2011). Emerging paradigms of β-arrestin-dependent seven transmembrane receptor signaling. Trends Biochem. Sci. *36*, 457–469.

Stallaert, W., Van Der Westhuizen, E.T., Schönegge, A.M., Plouffe, B., Hogue, M., Lukashova, V., Inoue, A., Ishida, S., Aoki, J., Le Gouill, C., et al. (2017). Purinergic receptor transactivation by the β2-adrenergic receptor increases intracellular Ca2+ in nonexcitable cells. Mol. Pharmacol. *91*, 533–544.

Stoeber, M., Jullié, D., Lobingier, B.T., Laeremans, T., Steyaert, J., Schiller, P.W., Manglik, A., and von Zastrow, M. (2018). A genetically encoded biosensor reveals location bias of opioid drug action. Neuron *98*, 963–976.e5.

Sutkeviciute, I., Clark, L.J., White, A.D., Gardella, T.J., and Vilardaga, J.P. (2019). PTH/PTHrP receptor signaling, allostery, and structures. Trends Endocrinol. Metab. *30*, 860–874.

Takasaki, J., Saito, T., Taniguchi, M., Kawasaki, T., Moritani, Y., Hayashi, K., and Kobori, M. (2004). A novel Gαq/11-selective inhibitor. J. Biol. Chem. *279*, 47438–47445.

Tsvetanova, N.G., and von Zastrow, M. (2014). Spatial encoding of cyclic AMP signaling specificity by GPCR endocytosis. Nat. Chem. Biol. *10*, 1061–1065.

Vilardaga, J.P., Gardella, T.J., Wehbi, V.L., and Feinstein, T.N. (2012). Non-canonical signaling of the PTH receptor. Trends Pharmacol. Sci. *33*, 423–431.

Wehbi, V.L., Stevenson, H.P., Feinstein, T.N., Calero, G., Romero, G., and Vilardaga, J.P. (2013). Noncanonical GPCR signaling arising from a PTH receptor-arrestin-Gβγ complex. Proc. Natl. Acad. Sci. U S A *110*, 1530–1535.

Wein, M.N., and Kronenberg, H.M. (2018). Regulation of bone remodeling by parathyroid hormone. Cold Spring Harb. Perspect. Med. *8*, a031237.

White, A.D., Fang, F., Jean-Alphonse, F.G., Clark, L.J., An, H.J., Liu, H., Zhao, Y., Reynolds, S.L., Lee, S., Xiao, K., et al. (2019). Ca2+ allostery in PTH-receptor signaling. Proc. Natl. Acad. Sci. U S A *116*, 3294–3299.

White, A.D., Jean-Alphonse, F.G., Fang, F., Peña, K.A., Liu, S., König, G.M., Inoue, A., Aslanoglou, D., Gellman, S.H., Kostenis, E., et al. (2020). Gq/11-dependent regulation of endosomal cAMP generation by parathyroid hormone class B GPCR. Proc. Natl. Acad. Sci. U S A *117*, 7455–7460.

STAR★METHODS

KEY RESOURCES TABLE

REAGENT or RESOURCE	SOURCE	IDENTIFIER
Antibodies		
Anti-PTHR1-Alexa Fluor 647 nanobody	Laboratory of Ross Cheloha, NIH	VHH_{PTHR}, described in (Cheloha et al., 2020a, 2020b)
Chemicals, peptides, and recombinant proteins		
Bafilomycin A1	Cayman Chemical	Cat# 11,038
Barbadin	MedChem Express	Cat# HY-119706
D-luciferin	Gold Bio	Cat# L-123-250
Dyngo-4a	Selleck Chem	Cat# S7163
FIPI	Cayman Chemical	Cat# 13,563
PLD1i	Laboratory of Alex Brown, Vanderbilt University	VU0359595
PLD2i	Laboratory of Alex Brown, Vanderbilt University	VU0364739
Phorbol 12-myristate 13-acetate (PMA)	Santa Cruz Biotechnology	Cat# sc-3576
PTH(1–34) (PTH)	GenScript	Cat# RP01001
PTH(1–34) Trp1 (PTH-Trp)	Massachusetts General Hospital Peptide/Protein Core Facility	Sequence: WVSEIQLMHNLGKH LNSMERVEWLRKKLQDVHNF-CO_2H
PTH-K13-TMR (PTH-TMR)	Massachusetts General Hospital Peptide/Protein Core Facility	Sequence: SVSEIQLMHNLGK(5-carboxytetramethylrhodamine) HLNSMERVEWLRKKLQDVHNF-CO_2H
YM-254890	Focus Biomolecules	Cat# 10-1590-0100
Critical commercial assays		
GloSensor cAMP responsive luciferase stably expressed in HEK 293	Promega	pGloSensor™-22F, # E2301, described in (Binkowski et al., 2011)
Experimental models: cell lines		
hPTHR1-HEK 293 containing GloSensor (293-PTHR1)	ATCC	CRL-11268 base cell line (HEK 293). Stable hPTHR1-HEK 293 expressing GloSensor plasmid originally described in (Maeda et al., 2013)
G_s KO-HEK 293 (G_s knockout achieved using CRISPR-Cas9)	Laboratory of Thomas Gardella, Harvard Medical School	G_s KO-HEK 293 cells, described in (Stallaert et al., 2017)
SaOS-2	ATCC	Cat#HTB-85, human osteosarcoma
SGS-72	ATCC	SaOS-2 cells stably expressing GloSensor (Cheloha et al., 2016)
UMR-106	ATCC	Cat#CRL-1661, Rat osteosarcoma
UGS-56	ATCC	UMR-106 cells stably expressing GloSensor (Daley et al., 2021)
Recombinant DNA		
hPTHR1-HA plasmid	Laboratory of Thomas Gardella, Harvard Medical School, custom plasmid (VectorBuilder). HA inserted into exon 2	Gardella lab plasmid #906
Software and algorithms		
ImageJ	NIH	https://imagej.nih.gov/ij/

RESOURCE AVAILABILITY

Lead contact

Further information and requests for resources and reagents should be directed to and will be fulfilled by the lead contact, Jeremy Baskin (jeremy.baskin@cornell.edu).

Materials availability

Materials generated in this study are available from the lead contact with a completed Materials Transfer Agreement.

Data and code availability

The published article includes all datasets generated or analyzed during this study.

EXPERIMENTAL MODEL AND SUBJECT DETAILS

Cell lines

HEK 293 cell lines (*H. sapiens*, embryonic kidney epithelial, female) that stably express human PTHR1 and cAMP GloSensor (293-PTHR1 cells) and HEK 293 G_s knockout cells that stably express GloSensor (i.e. G_s KO cells), osteosarcoma cell lines UMR-106 (*R. norvegicus*, adult, bone epithelial osteosarcoma, sex not available) and SaOS-2 (*H. sapiens*, 11 year old, bone epithelial osteosarcoma, female), and cell lines derived from these that stably express cAMP GloSensor UGS-56 (from UMR-106) and SGS-72 (from SaOS-2) were grown in DMEM (Dulbeccos modified Eagle medium) supplemented with 10% FBS and 1% penicillin/streptomycin and were maintained in a 5% CO_2, moisture-saturated atmosphere at 37°C. Cell densities were maintained between 10^5 and 1.6 x 10^6 cells/mL, and all cells were used between passages 20–40. For cell labeling experiments, all buffers or media were warmed to 37°C or room temperature prior to addition to cells unless otherwise noted, and incubations were done at 37°C unless otherwise specified.

METHOD DETAILS

General materials and methods

See key resources table for sources for reagents, cell lines, etc. All imaging experiments were performed on a Zeiss LSM 800 confocal laser scanning microscope equipped with 40X 1.4 NA Plan Apochromat objectives, 405, 488, 561, and 640 nm solid-state lasers, and two GaAsP PMT detectors, using the Zeiss Zen Blue 2.3 software. All image analysis was performed using FIJI/ImageJ. Flow cytometry experiments, except for Figures 1E and S1, was performed on a BD Accuri C6 flow cytometer, and analysis was performed using the BD Accuri C6 analysis software. Flow cytometry experiment for Figures 1E and S1 was performed on a Thermo Fisher Attune NxT Flow Cytometer equipped with 405, 488, 561, 637 nm lasers using 480 and 647 dual lasers. Luminescence measurements were performed using a Tecan Infinite M1000 Microplate Reader (cat # 30034301).

RT-IMPACT labeling with oxoTCO for live-cell imaging and flow cytometry analysis

HEK 293-PTHR1 cells or G_s KO cells (150,000 cells) were seeded on 35-mm glass-bottom imaging dishes (MatTek) for 24 hr prior to experiments. Rinses after oxoTCO incubation were performed in DMEM supplemented with FBS and P/S. Where indicated, the cells were then transfected with the indicated plasmid using Lipofectamine 2000 as per the manufacturer's instructions. One day after seeding (or transfection, if any), cells were first treated with the indicated PLD inhibitor (PLDi [FIPI], 750 nM; PLD1i [VU0359595], 250 nM; PLD2i [VU0364739], 350 nM; 30 min), YM-254890 (1 μM, 15 min), Dyngo-4a (30 μM, 15 min, serum-free), or corresponding DMSO vehicle in media at 37°C. The working concentrations of PTH(1–34) (PTH), PTH-Trp (Trp) and PTH-TMR were 50 nM and that of PMA was 100 nM. The appropriate stimulus was then added to the media for the indicated periods of time (0–20 min). Subsequently, freshly prepared oxoTCO (3 mM) together with the respective stimulus and PLD inhibitor/DMSO in media (100 μL) were carefully added to cover the central glass well.

Cautionary note: oxoTCOs are reported to have limited water stability (Lambert et al., 2017)*. Therefore, all aqueous oxoTCO solutions (e.g., those in DMEM-containing media) were used within 20 min of their generation. For example, we dissolved oxoTCO in 200 μL of DMEM with PLD inhibitor/DMSO and respective stimulus and used it only for two consecutive replicates rather than make a single stock solution for an entire day of experiments at the beginning of the day.*

The dish was incubated for 5 min, the treatment media was aspirated, the cells were rinsed with PBS (1 mL) briefly, and the cells were then rinsed in DMEM (500 μL) for 1 min at 37°C. The media was aspirated and replaced with Tz–BODIPY (0.33 μM) in PBS (100 μL) for 1 min, which was further aspirated and replaced with 100 μL Tyrode's-HEPES buffer. Cells were imaged immediately afterward. Multicolor images were obtained in two-channel, line-switching mode. Z stacks were taken with 0.45 μm sectioning. For flow cytometry analysis, cells were instead seeded in 24 well-plates (125,000 cells/well) and labeled as described above. Following the final aspiration of Tz–BODIPY, cells were lifted with trypsin, transferred to 96-well plates, rinse twice with cold PBS +0.5% FBS by centrifugation at 500 x g, and analyzed by flow cytometry. For the experiment shown in Figure 1E, an extra step of incubation of anti-PTHR1-Alexa Fluor 647 nanobodies (100 nM) at 4°C in the dark for 30 min before oxoTCO incubation steps. At least 10,000 live cells were analyzed for each well in all flow cytometry experiments, as determined by forward/side scatter analysis for all experiments and additional gating for the experiment shown in Figure 1E (see Figure S1).

For Figures S4B–S4D, IMPACT labeling for flow cytometry analysis (Bumpus et al., 2020) was performed as described above but substituting azidopropanol (10 mM) and BCN-BODIPY (1 mM) in place of oxoTCO in place of Tz-BODIPY, respectively, and with the BCN-BODIPY incubation being 10 min followed by 10 min rinse-out in full media at 37°C. Phorbol 12-myristate 13-acetate (PMA, 100 nM), where indicated, was added to the cells together with azidopropanol with no prior incubation as a positive control for PLD activation. Barbadin (100 μM, serum-free), where indicated, was present 30 min before experiment. The incubation of

BCN-BODIPY was performed at 37°C for 10 min followed by rinsing in Tyrode's-HEPES buffer at 37°C for 10 min and triple rinses in PBS prior to trypsinization.

Luciferase assays of cAMP production

Procedures were adopted from previously published protocols (Cheloha et al., 2014). Monolayers of HEK 293 cells stably expressing PTHR1 were seeded on a 96-well plate 24 hr before experiments. Dyngo-4a (30 μM) or corresponding DMSO vehicle, where indicated, was incubated with the cells in serum-free media for 15 min at 37°C prior to the experiment. The cells were incubated with D-luciferin (0.5 mM) for 30 min at room temperature until the luminescence achieved a steady baseline. PTH ligands (50 nM) were then added to the wells and luminescence recorded by a Tecan Infinite M1000 Microplate Reader at the indicated time points.

Imaging of PTH-TMR to visualize PTHR1 endocytosis

293-PTHR1 cells (150,000 cells) were seeded on 35-mm glass-bottom imaging dishes (MatTek) for 24 h prior to experiments. Dyngo-4a (30 μM), where indicated, was incubated with the cells in serum-free media for 15 min at 37°C prior to the experiment. PTH-TMR (50 nM) was added to cells for 20 s, followed by three PBS rinses and imaging, with excitation by the 561 nm laser.

RT-IMPACT imaging of the localization of PLD activity

Real-time IMPACT using oxoTCO ((*S*)-oxoTCO–C1) and Tz-BODIPY was performed as described previously (Bumpus et al., 2020; Liang et al., 2019). Briefly, freshly prepared oxoTCO (3 mM) together with the PTH(1–34) or PTH-TMR (50 nM) in media (100 μL) were carefully added to cover the central glass well. The dish was incubated for 5 min, the treatment media was aspirated, the cells were rinsed with PBS (1 mL) briefly, and the cells were then rinsed in DMEM (500 μL) for 1 min at 37°C. The media was replaced with 100 μL of Tyrode's-HEPES buffer to cover the center of the glass bottom and the dish was mounted on the microscope. The cells to be imaged were quickly located, and time-lapse imaging with an interval of 3 s (488 nm, for PTH(1–34) or 6 s (488 nm and 561 nm, for PTH-TMR) and duration of 3 min was begun. Tz-BODIPY (100 μL, 1 μM in PBS) was added dropwise but quickly to the center of the dish during acquisition. The image shown in Figure 2B represents the 9-s time point post-addition of Tz-BODIPY. The RT-IMPACT experiment was repeated four times, yielding similar localizations.

QUANTIFICATION AND STATISTICAL ANALYSIS

All imaging experiments show representative images from experiments performed in at least three biological replicates on different days, where each replicate refers to a single dish of cells with approximately 15 cells in the field of view, whose parameters were all determined and averaged for the data point for that dish. Exact numbers of replicate experiments, sample sizes, and p values are provided in each figure legend. For experiments involving quantification of comparisons between more than two independent groups, significance was calculated using one-way ANOVA, followed by Games-Howell post-hoc test (for samples of unequal variance).